Engineering Fracture Mechanics 273 (2022) 108731

Contents lists available at ScienceDirect

Engineering Fracture Mechanics

journal homepage: www.elsevier.com/locate/engfracmech

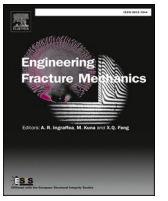

Atomistic scale behaviors of intergranular crack propagation along twist grain boundary in iron under dynamic loading

Zhifu Zhao [a,b,c,*], Babak Safaei [d], Yanfei Wang [b], Yanwei Liu [b], Fulei Chu [c], Yueguang Wei [b]

[a] LNM, Institute of Mechanics, Chinese Academy of Sciences, Beijing 100190, PR China
[b] Department of Mechanics and Engineering Science, College of Engineering, Peking University, Beijing 100871, PR China
[c] Department of Mechanical Engineering, Tsinghua University, Beijing 100084, PR China
[d] Department of Mechanical Engineering, Eastern Mediterranean University, Famagusta, North Cyprus via Mersin 10, Turkey

ARTICLE INFO

Keywords:
Dynamic load
Molecular dynamics
Intergranular crack propagation
Stacking fault
Dislocation

ABSTRACT

Due to alternative exchange between single and double-teeth meshings, the upper part of gear tooth is subjected to dynamic tensile stress whose growth rate presents rectangular fluctuation. This work investigates the atomistic scale behaviors of intergranular crack propagation along twist grain boundary in body-centered cubic (bcc) iron under dynamic tensile stress. The effects of driving force and contact ratio are fully discussed. Results show that only stacking faults with face-centered cubic (fcc) atoms can be formed in lower monocrystal portion. Edge dislocations in upper monocrystal portion are suppressed by intergranular crack cleavage. Critical stresses for stacking fault nucleation and intergranular crack cleavage vary with driving force and contact ratio. By calculating actual stress intensity factor at crack tip, variations of critical stresses are found to be attributed to the variations of time-dependent factors. Although critical stresses vary with driving force and contact ratio, the effects of these factors on the growths of crack length and plastic zone are not obvious in the early stage of intergranular crack propagation. Accumulated plastic strain energy before intergranular crack cleavage is independent of driving force and contact ratio. Departing from the early stage, the growth rates of crack length and plastic zone increase significantly with an increase in driving force or a decrease in contact ratio. However, the final ductile level of intergranular crack propagation cannot vary with contact ratio and large driving force. By applying dynamic load, this work can be used to reveal the atomistic scale mechanism of gear failure. The results can provide a good reference for gear safety design.

1. Introduction

As an efficient equipment used for the transformation of wind energy, wind turbine has obtained extensive application. Gear transmission system is the core of wind turbines, and its failure is the main threat to downtime accident [1]. As a typical gear failure, tooth breakage is in fact attributed to micro crack initiation and propagation. To identify the mechanisms of crack initiation and propagation, fracture mechanics based on continuum concept is generally applied [2]. Gear material is usually treated as an isotropic continuum. However, gear teeth are subjected to cyclic meshing force, and the amount of crack growth during a meshing cycle is at

* Corresponding author at: LNM, Institute of Mechanics, Chinese Academy of Sciences, Beijing 100190, PR China.
E-mail addresses: zhaozf@pku.edu.cn, zhaozhifu@imech.ac.cn (Z. Zhao).

https://doi.org/10.1016/j.engfracmech.2022.108731
Received 19 July 2021; Received in revised form 31 July 2022; Accepted 16 August 2022
Available online 20 August 2022

Nomenclature

Å	Length unit
A_0, B_0	Atoms used to determine hypothetical sharp right crack tip
A_1, B_1	Atoms used to determine real right crack tip
AB, BC, CD	First double-teeth, single-tooth, and second double-teeth meshing areas
C_1, C_2	Elastic coefficients of upper and lower monocrystal portions
E	Elastic modulus
E_g	Grain boundary energy
eV	Energy unit
f_I	Dynamic time-dependent factor
F	Tensile force on simulation model
F_1, F_2	Meshing forces during double-teeth and single-tooth meshing
F_I	A factor determined by the model geometry parameters
GPa	Stress unit
K_G	Critical Griffith stress intensity factor for intergranular crack cleavage
K_G^A	Critical stress intensity factor for cleavage in ductile propagation way
$K_I(t)$	Dynamic stress intensity factor induced by dynamic mode I loading
l_{CX}	Crack length
L_X, L_Y, L_Z	Model lengths along X, Y, and Z axes
M	Bending moment
N	Number of atoms on crack upper surface
P	Number of atoms on crack lower surface
ps	Time unit
r_1, r_2	Distances to right and left tips
s	Contact ratio
t	Time
T	Meshing period
u_y	Vertical displacement
u_{yu}	Vertical displacement of crack upper surface
u_{yl}	Vertical displacement of crack lower surface
x_i	X axis value of the ith atom on crack upper surface
x_j	X axis value of the jth atom on crack lower surface
α	Model geometry parameter,$\alpha = l_{CX}/L_X$
β	Model geometry parameter,$\beta = L_Y/L_X$
γ	Free surface energy
γ_p	Accumulated plastic strain energy before crack cleavage
θ_1,θ_2	Angles determined by respective radius vector and X axis
ν	Poisson ratio
$\sigma(t)$	Applied dyanmic tensile stress
ΔE	Total energy increment
$\Delta E_{\text{elastic}}$	Elastic strain energy increment
$\Delta E_{plastic}$	Plastic strain energy increment
$\Delta E_{surface}$	Crack surface energy increment
ΔQ	Heat dissipation increment

atomistic scale [3]. At atomistic scale, gear material is considered as many discrete iron atoms with body-centered cubic (bcc) crystal structure. These discrete iron atoms can form a great number of randomly orientated grains. Anisotropy and micro structure, like grain boundary, need to be taken into consideration.

Due to the strong anisotropy of bcc iron at atomistic scale, crack propagation behavior depends heavily on crystallographic orientation. On the one hand, free surface energy is determined by the crystal plane index of surface and is a key parameter in the evaluation of fracture toughness [4]. Therefore, fracture toughness that measures brittle crack cleavage ability depends on the crystal direction of crack plane [5]. On the other hand, plastic behavior derives from atomic slip, and atomic slip characteristic is determined by the angle between slip plane and crack plane, complement angle between slip direction and crack front, unstable stacking fault energy, and unstable twinning energy [6–7]. Specifically, the angle between slip plane and crack plane, complement angle between slip direction and crack front, and unstable stacking fault energy determine leading partial dislocation nucleation ability [6]. Unstable stacking fault energy and unstable twinning energy determine whether perfect dislocation or twinning is formed [7]. For cracks with different plane or front directions, the angle between slip plane and crack plane, complement angle between slip direction and crack

front, unstable stacking fault energy, and unstable twinning energy are very disparate. Hence, the nucleation ability and type of plastic behavior depend on the directions of crack plane and front [8–17]. Fracture toughness and plastic behavior nucleation ability determine the ductile–brittle characteristic of crack propagation.

Difference in crystallographic orientation between two single crystals leads to the appearance of grain boundary. Grain boundary is the main micro structure of crystalline material and plays a major role in fracture behavior. Available researches show that crystalline materials prefer intergranular fracture [18–20]. According to the orientation relationship between two single crystals, grain boundary can have tilt and twist forms, where tilt grain boundary can be symmetrical or asymmetrical [20]. Researchers have applied molecular dynamics theory to investigate intergranular crack propagation behavior along symmetrical tilt grain boundary, where the effect of grain boundary structure is discussed [21–26]. Although single crystal portions on both sides of symmetrical tilt grain boundary have different crystallographic orientations, their inner atoms are distributed symmetrically along grain boundary. Two single crystal portions have the same plastic behavior nucleation ability and type due to their identical atomic slip characteristic. Different from the case of symmetrical tilt grain boundary, atoms inside two single crystal portions are usually distributed asymmetrically along the twist grain boundary. Two single crystal portions can have different plastic nucleation abilities and types due to their disparate atomic slip characteristics. Therefore, it is necessary to identify the behaviors of intergranular crack propagation along twist grain boundary.

With gear transmission, a gear tooth is subjected to dynamic meshing force during a meshing cycle. Molecular dynamics studies carried out under quasi-static loading cannot be used to analyze the crack initiation and propagation mechanisms of service engineering components and structures subjected to dynamic load [8–12,14–17,21–26]. Studies carried out under cyclic [27–30] and impact [31] loadings have illustrated the feasibility of discussing time-variant loading effect through molecular dynamics simulation. Hence, the authors of this work have applied molecular dynamics to simulate crack initiation and propagation in monocrystal bcc iron under dynamic load induced by dynamic meshing force [13,32–33]. Due to the significant effect of grain boundary on crack propagation behavior at atomistic scale, this work mainly focuses on the intergranular crack propagation along twist grain boundary in bicrystal bcc iron under dynamic load. The results of this work can better explain the atomistic scale engineering mechanism of tooth breakage.

2. Model and methods

According to previous studies [13,32–33], a gear tooth can experience one single-tooth meshing period (BC) and two double-teeth meshing periods (AB and CD) during a meshing cycle, as described in Fig. 1(a). Single tooth meshing period is (2-*s*)*T*, and each double-teeth meshing period is (*s*-1)*T*, where *s* and *T* are contact ratio and entire meshing period, respectively. During single-tooth meshing, driving force is supported by one tooth of each gear, while during double-teeth meshing, driving force is supported by two teeth of each gear. As a result, meshing force on gear tooth during single-tooth meshing is much higher than that during double-teeth meshing. Dynamic and moving meshing force can result in a dynamic bending moment with rectangular growth rate. Under this dynamic bending moment, the upper part of gear tooth is subjected to tensile stress. Similar to the variation of dynamic bending moment, the growth rate of this tensile stress also presents rectangular fluctuation, and its value during single-tooth meshing is higher than that during double-teeth meshing. Therefore, this work mainly focuses on intergranular crack propagation under dynamic load whose growth rate presents rectangular fluctuation.

In bcc iron, the atomic close-packed planes belonging to the cluster of {1 1 0} have the lowest surface free energy [4]. The propagation behaviors of cracks along the {1 1 0} planes and along the grain boundaries formed by {1 1 0} planes need to be investigated. Previous studies [13,32] by the authors in this work have shown that the crack with the front of [0 $\bar{1}$ 0] has a low threshold for plastic behavior nucleation while the crack with the front of [10 $\bar{1}$] has a high threshold for plastic behavior nucleation when propagating along the (101) plane. Besides, the generated stacking faults have weak resistance to the (101) [0 $\bar{1}$ 0] crack growth, but the nucleated dislocations have strong resistance to the (101) [10 $\bar{1}$] crack growth. The two single crystals containing (101) [0 $\bar{1}$ 0]

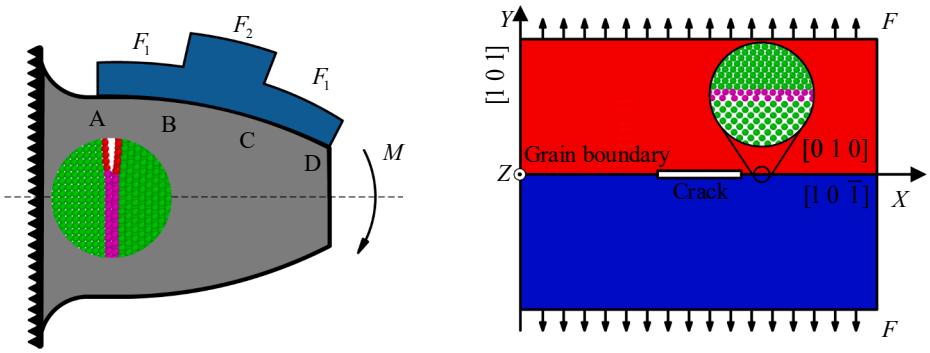

(a) Dynamic load induced by gear engagement. (b) Molecular dynamics simulation model

Fig. 1. Molecular dynamics simulation.

and (101) [10 $\bar{1}$] cracks have different orientations. The significant differences in plastic behavior nucleation and crack growth resistance make the propagation behavior of crack along the twist grain boundary formed by these two single crystals more confusing. As shown in Fig. 1(b), a bicrystal bcc iron model containing the twist grain boundary and a pre-existing central crack is developed, where the twist axis is along [101] crystal direction. The axes X, Y, and Z are along [010], [101], and [10 $\bar{1}$] crystal directions for upper monocrystal portion and along [10 $\bar{1}$], [101], and [0 $\bar{1}$ 0] crystal directions for lower monocrystal portion. Simulation model has the $L_X \times L_Y \times L_Z$ dimensions of 1034 Å×727 Å×20 Å, and two monocrystal portions have the same length along twist axis. Pre-existing crack is realized by turning off pairwise interactions between certain pairs of atoms, and its length l_{CX} is 84.2 Å.

After modelling, molecular dynamics simulations are performed in the environment of LAMMPS [34]. The widely used atomic potential that is developed by Mendelev et al. [35] on the basis of the embedded-atom method is applied to describe the interactions between bcc iron atoms. The physical properties such as lattice parameter, point-defect energies, elastic constants, bcc–fcc transformation energy, liquid structure factor, liquid density and melting temperature determined by this atomic potential are in good agreement with those obtained by diffraction experiments or first-principles calculations. The velocity Verlet algorithm [36] is used to

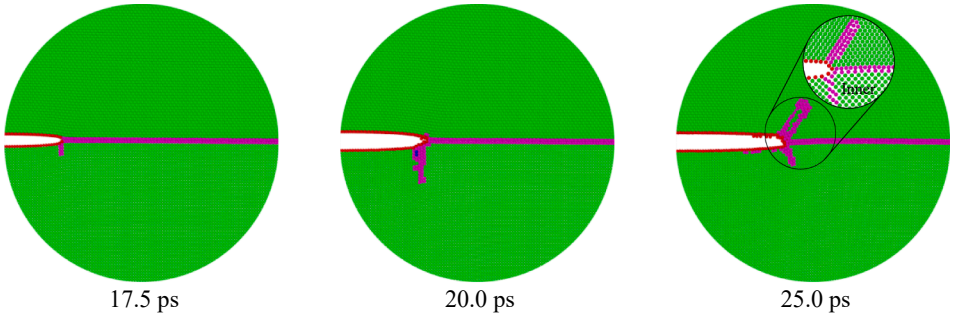

(a) Bicrystal

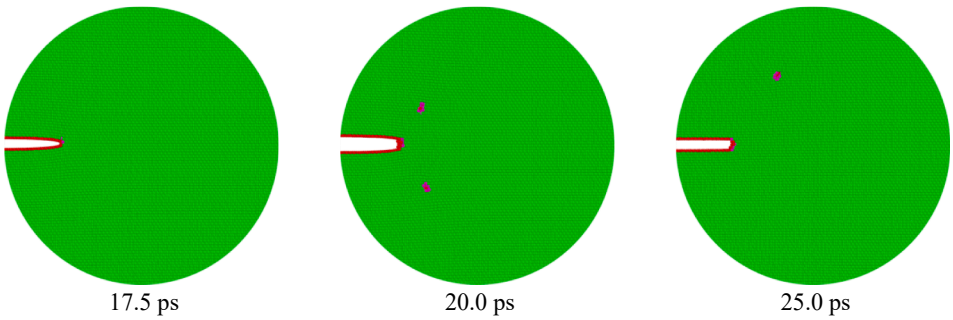

(b) Monocrystal I

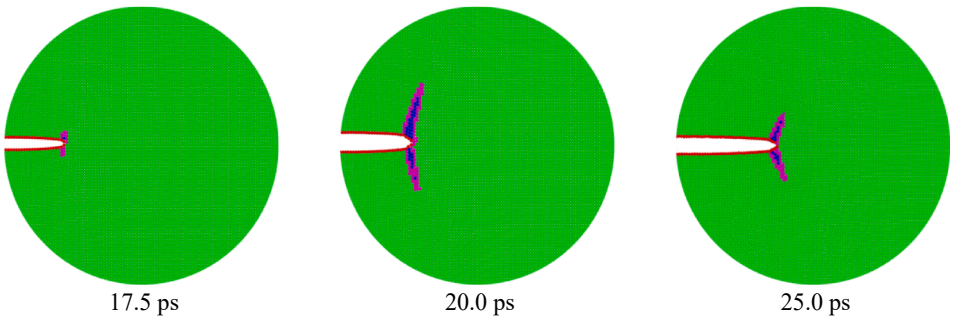

(c) Monocrystal II

Fig. 2. Crack propagation behaviors in bicrystal and monocrystals I and II, where the pink atoms are located at grain boundaries and dislocation cores, red atoms are located at crack surface, green atoms have bcc crystal structure, and blue atoms have fcc crystal structure.

calculate the atomic position and velocity vectors at every timestep by integrating the Newton's equations of motion. During simulation, the model undergoes the processes of equilibration and stretching after setting the initial velocities of atoms. The initial velocities of atoms and the equilibration process are the same as those reported in previous studies [13,32–33]. The stretching process is carried out 25 ps under microcanonical ensemble by applying dynamic tensile force along *Y* direction, where the timestep is 0.001 ps. As in previous studies [13,32–33], free boundaries are applied along both *X* and *Y* directions to shrink and stretch the model freely, and periodic boundaries are applied along *Z* direction to avoid surface effect.

3. Result analysis

3.1. Intergranular crack propagation behavior

As illustrated by Curtin [17] and Gao [21], intergranular crack propagation behavior is determined by resistances against crack cleavage and plastic behavior nucleation. According to previous studies [13,33], thresholds for plastic behavior nucleation in upper and lower monocrystal portions are 0.954 and 0.663 MPa·m$^{1/2}$, respectively. Threshold for intergranular crack cleavage can be calculated as.

$$K_G = \sqrt{2(2\gamma - E_g)/(C_1 + C_2)} \tag{1}$$

where free surface energy γ and grain boundary energy E_g are 1.650 and 0.64 J/m^2, respectively. The variables of C_1 and C_2 are elastic coefficients of upper and lower monocrystal portions, respectively. Based on a previous study [13], the elastic coefficients of C_1 and C_2 are calculated as 3.9×10^{-12} and 4.7×10^{-12} m^2/N. Thus, threshold for intergranular crack cleavage can be computed to be 0.787 MPa·m$^{1/2}$.

A molecular dynamics simulation on bicrystal model is first performed under dynamic tensile stress whose contact ratio is 5/3 and growth rates during double-teeth (AB and CD) and single-tooth (BC) meshings are 0.25 and 0.5 GPa/ps, respectively. To identify intergranular crack propagation behavior along twist grain boundary, molecular dynamics simulations on crack propagation in two monocrystals are carried out under the same dynamic tensile load as bicrystal case. Two monocrystal simulation models and their internal cracks have the same dimensions as bicrystal model and its internal crack, respectively. Atomic structure [37] and potential are calculated to recognize the evolutions of plastic behavior and crack surface. As shown in Fig. 2(b) and (c), edge dislocations with slip systems of $(1\ \bar{2}\ 1)[111]$ and $(\bar{1}\ \bar{2}\ \bar{1})[\bar{1}\ 1\ \bar{1}]$ can be nucleated at crack tip in monocrystal I, and stacking faults containing face-centered cubic (fcc) atoms can be formed at crack tip in monocrystal II. The leading partial dislocations of edge dislocation and stacking fault are nucleated before crack cleavage. Crack propagations in two monocrystals are ductile. Since the threshold for stacking fault nucleation is lower than that for intergranular crack cleavage, stacking faults containing fcc atoms can be formed first in lower monocrystal portion whose crystal orientation is the same as monocrystal II, as described in Fig. 2(a). After stacking fault formation, intergranular crack starts to cleave, and edge dislocations cannot be observed in the upper monocrystal portion whose orientation is the same as that of monocrystal I. Since the threshold for edge dislocation nucleation is higher than that for intergranular crack cleavage, edge dislocations are suppressed by intergranular crack cleavage. Although edge dislocation nucleation is suppressed, atomic slip can occur in upper monocrystal portion once the applied load exceeds the threshold for anti-twinning nucleation. As depicted in Fig. 2(a), atomic slip in upper monocrystal portion can lead to the formation of anti-twinning bands at crack tip. These anti-twinning bands are unstable because their thickness is decreased on some inner atomic planes vertical to crack front direction. Because anti-twinning bands are formed after intergranular cleavage, they cannot contribute to inherent ductile way of intergranular crack propagation. Inherent ductile propagation way is only attributed to stacking fault formation in lower monocrystal portion.

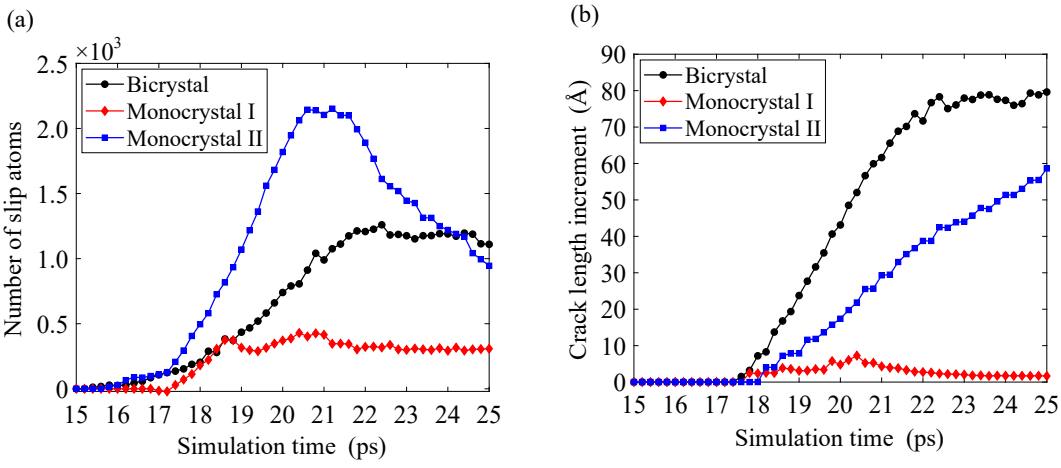

Fig. 3. Quantitative description of intergranular crack propagation, where (a) is the number of slip atoms and (b) is crack length increment.

To quantitatively describe intergranular crack propagation behavior, Fig. 3(a) and (b) show the changes in the number of slip atoms and crack length, respectively. As shown in Fig. 3(a), stacking faults with fcc atoms are almost simultaneously formed in monocrystal II and bicrystal. Grain boundary has little effect on the threshold for stacking fault formation in lower monocrystal portion. Different from stacking fault formation, grain boundary can significantly decrease threshold for brittle crack cleavage. As shown in Fig. 3(b), crack cleaves in monocrystal II later than that in monocrystal I. Due to $C_2 > C_1$, threshold for brittle crack cleavage in monocrystal II is lower than that for brittle crack cleavage in monocrystal I. Stacking fault formation inhibits crack cleavage in monocrystal II. Similar to crack propagation in monocrystal II, stacking faults can also be formed in bicrystal. However, cracks almost simultaneously cleave in bicrystal and monocrystal I. In particular, crack cleaves in bicrystal much earlier than that in monocrystal II. Hence, threshold for intergranular brittle crack cleavage is much lower than that for brittle crack cleavage in monocrystals.

Propagating with the velocity of 6266 m/s along the direction of [101], the heavy load of single-tooth meshing arrives at crack tip at 15.8 ps and terminates at 20.8 ps. During single-tooth meshing, the number of slip atoms increases moderately in monocrystal I, which means that edge dislocations can be continuously nucleated and emitted from crack tips. Dislocation nucleation and emission blunt crack tips, so crack grows slowly. Crack propagation in monocrystal I is strong ductile. Besides, one can find that the growth rate of the number of slip atoms in bicrystal is about half that in monocrystal II, but the growth rate of crack length is about twice. Hence, crack propagation in monocrystal II is more ductile than in bicrystal. Intergranular crack propagation occurs in the weakest ductile way under heavy load during single-tooth meshing.

Different from single-tooth meshing, simulation model is subjected to slight load during second double-teeth meshing. As shown in Fig. 3(b), intergranular crack length and the number of slip atoms are almost invariant during second double-teeth meshing, which is similar to the case of monocrystal I but different from monocrystal II. In monocrystal II, crack still grows, but the number of slip atoms decreases. Stacking faults shrink with crack growth, and crack propagation transforms from ductile to brittle. Although crack cannot grow in bicrystal during second double-teeth meshing, its final length is still much longer than that in monocrystal II. Intergranular crack propagation is still not as ductile as crack propagation in monocrystal II. Since crack propagation in monocrystal I is in a strong ductile way with dislocation movement, intergranular crack propagation is still in the weakest ductile mode.

3.2. *Intergranular crack propagation mechanism*

With intergranular crack propagation, both crack new surface formation and plastic slip band extension need to absorb energy. Intergranular crack propagation behavior is closely related to energy variation. According to a previous study [33], one can have.

$$\Delta E - \Delta Q - \Delta E_{\text{elastic}} = \Delta E_{\text{plastic}} + \Delta E_{\text{surface}} \tag{2}$$

whereΔE,ΔQ,$\Delta E_{\text{elastic}}$,$\Delta E_{\text{plastic}}$, and $\Delta E_{\text{surface}}$ are the increments of total energy, heat dissipation, elastic strain energy, plastic strain energy, and crack surface energy, respectively. In this work, plastic strain energy increment is the sum of potential energy increments of all atoms located at dislocation cores, twinning boundaries, and stacking faults. Crack surface energy increment is the sum of potential energy increments of all atoms located at crack surface.

Fig. 4 depicts the variation of the sum of plastic strain and crack surface energy increments which are zero at 15.0 ps. The variation of the sum of plastic strain and crack surface energy increments in bicrystal is similar to that in monocrystal II. As illustrated in section 3.1, during single-tooth meshing, intergranular crack growth is much faster than crack growth in monocrystal II, but the number of slip atoms in bicrystal is much less than that in monocrystal II due to the suppression of edge dislocation in the upper monocrystal portion of bicrystal. Without competing with plastic behavior in upper monocrystal portion, intergranular crack can absorb more energy to form new surfaces. Even though the variations of the sum of plastic strain and crack surface energy increments in bicrystal and monocrystal II are similar, intergranular propagation has higher crack surface energy. Extra crack surface energy in bicrystal is derived

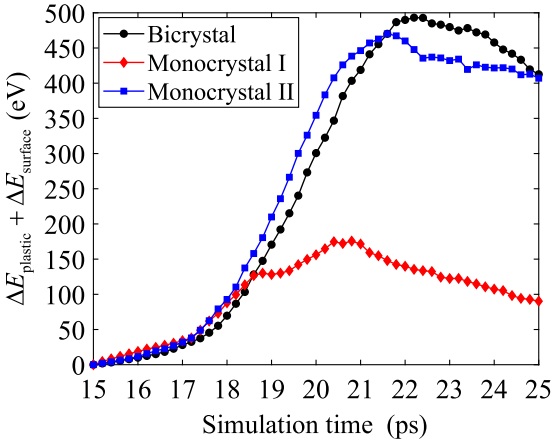

Fig. 4. Variation of the sum of plastic strain and crack surface energy increments.

from the energy which should have been absorbed by atomic slip to form plastic behavior in upper monocrystal portion of bicrystal. During second double-teeth meshing, the sum of plastic strain and crack surface energies decreases in bicrystal, monocrystal I, and monocrystal II. The decrement of the sum of plastic strain and crack surface energies in bicrystal is about the same as that in monocrystal I, but is higher than that in monocrystal II. The less decrement of the sum of plastic strain and crack surface energies in monocrystal II indicates that crack new surface energy is derived from the decrease of plastic strain energy. However, crack tip cannot move forward in bicrystal and monocrystal I. Hence, plastic strain energy is dissipated and cannot contribute to crack new surface formation. In monocrystal I, plastic strain energy is dissipated by edge dislocation movement. In bicrystal, plastic strain energy is dissipated by anti-twinning extension along atomic slip direction.

4. Discussions

4.1. Effect of driving force on intergranular crack propagation

Driving force determines the growth rate of tensile stress on the upper part of gear tooth root at each meshing area. Inconstant driving force is a typical characteristic of gear transmission. For example, the driving force of gears in wind turbines varies with wind speed. With driving force increase, the growth rate of tensile stress at each meshing area increases. To identify the effect of driving force on intergranular crack propagation, five comparative simulations with the same contact ratio of 5/3 are conducted. In these five comparative simulations, loading rates at double-teeth (single-tooth) meshing area are 0.30 (0.60) GPa/ps, 0.35 (0.70) GPa/ps, 0.40 (0.80) GPa/ps, 0.45 (0.90) GPa/ps, and 0.50 (1.00) GPa/ps.

4.1.1. Engineering stress–strain behavior

Fig. 5 describes the engineering stress–strain behaviors of cracked bicrystal model under different loading rates. These engineering stress–strain curves overlap in their quasi-linear parts. As a consequence, bicrystal model can be seen to be subjected to yielding when each engineering stress–strain curve starts to deviate from its quasi-linear part. Points ‘a’ to ‘f’ indicate the moments when stress–strain curve deviates from its quasi-linear part under different loading rates. Corresponding stress at these points can be seen as yield stress. With an increase in loading rate, yield stress increases in a nonlinear way, as shown by the black curve with solid circles in Fig. 6. The nonlinear variation of yield stress with loading rate puts forward high requirements for the safety design of gears, especially under heavy load working conditions. After deviating from quasi-linear part, bicrystal model is subjected to plastic deformation. Under the loading rate of 0.25 (0.50) GPa/ps, elastic retraction performance can be observed at the end of stress–strain curve. However, under the loading rates of higher than 0.25 (0.50) GPa/ps, elastic retraction performance cannot be observed, and the bicrystal model can be stretched further after stress reaches its maximum. Therefore, under the loading rates of higher than 0.25 (0.50) GPa/ps, maximum tensile stress on engineering stress–strain curve represents the ultimate strength of cracked bicrystal model. As shown in Fig. 5, ultimate strength also increases with an increase in loading rate.

4.1.2. Early crack propagation and its correlation with yielding

In the early stage of intergranular crack propagation, stacking faults are nucleated before crack cleavage. As shown by blue curve with squares in Fig. 6, critical stress for intergranular crack cleavage also increases with an increase in loading rate in a nonlinear way, which is similar to the variation of yield stress. Different from the variations of yield stress and critical stress for intergranular crack cleavage, critical stress for stacking fault nucleation moderately increases with an increase in loading rate only when loading rate is lower than 0.45(0.90) GPa/ps, as shown by red curve with diamonds in Fig. 6. When loading rate is higher than 0.45(0.90) GPa/ps, critical stress for stacking fault nucleation decreases with further increase of loading rate. Based on Fig. 6, one can conclude that the

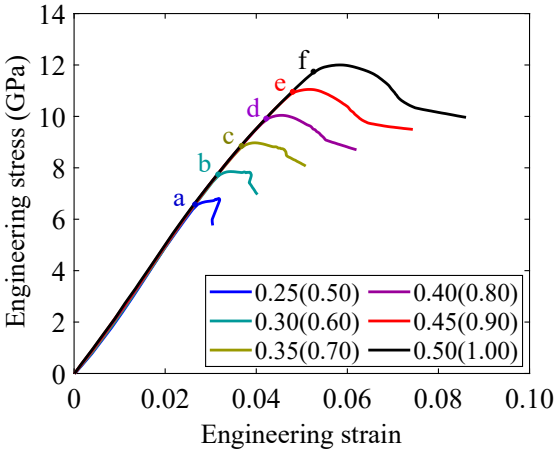

Fig. 5. Effect of driving force on engineering stress–strain behavior.

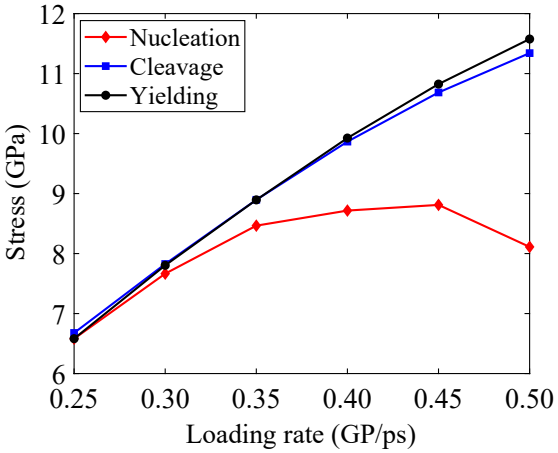

Fig. 6. Variations of yield stress, critical stress for intergranular crack cleavage, and critical stress for stacking fault nucleation with loading rate.

curve of critical stress for intergranular crack cleavage intersects with the curve of yield stress. At the point of intersection, loading rate at double-teeth (single-tooth) meshing area is about 0.35 (0.70) GPa/ps. Hence, under loading rates of lower than 0.35 (0.70) GPa/ps, critical stress for intergranular crack cleavage is higher than yield stress. Intergranular crack cleaves after bicrystal model yields. However, under loading rates of higher than 0.35 (0.70) GPa/ps, critical stress for intergranular crack cleavage is lower than yield stress. Intergranular crack cleaves before bicrystal model yields. Compared with yield stress, the nonlinear variation of critical stress for intergranular crack cleavage with loading rate puts forward higher requirements for the safety design of gears under heavy load working conditions. Besides, one can conclude that critical stress for stacking fault nucleation is always lower than yield stress. Stacking fault formation and evolution are essential factors leading to yield. With an increase in loading rate, the difference between critical stress for stacking fault nucleation and yield stress increases. Hence, gears are very dangerous under larger driving forces. Stacking faults are easily nucleated under heavy load working conditions. To provide a good reference for gear safety design, the mechanisms of the variation of critical stress for stacking fault formation and the variation of critical stress for intergranular crack cleavage need to be identified.

In fracture mechanics framework, crack propagation is controlled by stress intensity factor. As reported in Machová [31] and a previous study [32], dynamic load can lead to a dynamic stress intensity factor through a dynamic time-dependent factor.

$$K_I(t) = F_I(\alpha,\beta) f_I(\alpha,\beta,\sigma)\sigma(t)\sqrt{\pi l_{CX}/2} \tag{3}$$

where F_I is the factor determined by the model geometry parameters of α andβ. These parameters can be calculated as $\alpha = l_{CX}/L_X$ and$\beta = L_Y/L_X$, respectively. For the developed bicrystal model in this work, geometry factor F_{I} is calculated as 1.02 on the basis of Murakami [38]. Dynamic time-dependent factor f_{I} has a significant effect on crack propagation by enhancing or weakening applied stress. To obtain dynamic time-dependent factor, Eq. (3) can be rewritten as

$$f_I = \frac{K_I(t)}{F_I(\alpha,\beta)\sigma(t)\sqrt{\pi l_{CX}/2}} \tag{4}$$

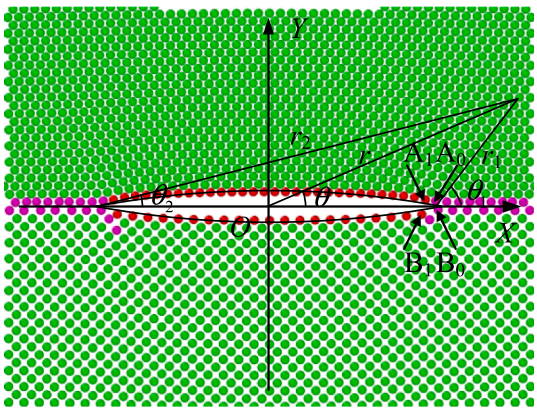

Fig. 7. Crack opening profile.

Based on normal stress in front of crack tip and linear extrapolation with least square, dynamic stress intensity factor for monocrystal model has been calculated to obtain the dynamic time-dependent factor in the previous study [32]. However, for bicrystal model, there are stress concentrations at crack tip and interface dislocations. Normal stress in front of crack tip is oscillatory, as shown in Fig. A1. Corresponding precise dynamic stress intensity factor is difficult to be calculated based on oscillatory normal stress. To calculate precise dynamic stress intensity factor for bicrystal model, a method based on crack opening profile is proposed in this work. For an ideal sharp central pre-existing crack in isotropic material, vertical displacement u_y under plain strain condition and pure mode I loading can be calculated as [39].

$$u_y = \frac{2(1-\nu^2)K_I(t)\sqrt{r_1 r_2}\sin[(\theta_1+\theta_2)/2]}{E\sqrt{\pi l_{CX}/2}} \tag{5}$$

where ν and E are Poisson's ratio and elastic modulus, respectively. As shown in Fig. 7, variables r_1 and r_2 are distances to right and left tips, respectively. Variables θ_1 and θ_2 are the angles determined by respective radius vector and X axis, respectively. For crack upper surface, one can have $\theta_1 = \pi$ and$\theta_2 = 0$. The corresponding displacement can be computed as

$$u_{yu} = \frac{2(1-\nu^2)K_I(t)\sqrt{r_1 r_2}}{E\sqrt{\pi l_{CX}/2}} \tag{6}$$

For crack lower surface, one can have $\theta_1 = -\pi$ and$\theta_2 = 0$. The corresponding displacement can be calculated as.

$$u_{yl} = -\frac{2(1-\nu^2)K_I(t)\sqrt{r_1 r_2}}{E\sqrt{\pi l_{CX}/2}} \tag{7}$$

At atomistic scale, ideal sharp crack tips cannot exist even though pairwise interaction is turned off without deleting any atomic layer. As described in Fig. 7, a real right crack tip is determined by the atoms designated by A_1 and B_1, and a hypothetical sharp right crack tip is determined by the atoms designated by A_0 and B_0. Ideal sharp right crack tip is defined by the middle point between A_0 and B_0 atoms.

For anisotropic bicrystal material, one can have.

$$C_1 + C_2 = \frac{2(1-\nu^2)}{E} \tag{8}$$

If coordinate origin changes from O to ideal sharp right crack tip, dynamic stress intensity factor can be calculated as.

$$K_I(t) = \frac{1}{2(C_1+C_2)}\left[\frac{1}{N}\sum_{i=1}^{N}\frac{u_{yu}^i\sqrt{\pi l_{CX}/2}}{\sqrt{-x_i l_{CX}-x_i^2}} + \frac{1}{P}\sum_{j=1}^{P}\frac{-u_{yl}^j\sqrt{\pi l_{CX}/2}}{\sqrt{-x_j l_{CX}-x_j^2}}\right] \tag{9}$$

where x_i is the X axis value of the ith atom on crack upper surface, x_j is the X axis value of the jth atom on crack lower surface, N is the number of atoms on crack upper surface, and P is the number of atoms on crack lower surface. As shown in Fig. 8, calculated dynamic stress intensity factor can well reflect simulated crack opening profile. Intergranular crack propagation can be considered to be controlled by the calculated dynamic stress intensity factor.

Based on Eqs. (4) and (9), one can calculate dynamic time-dependent factor for anisotropic bicrystal material as.

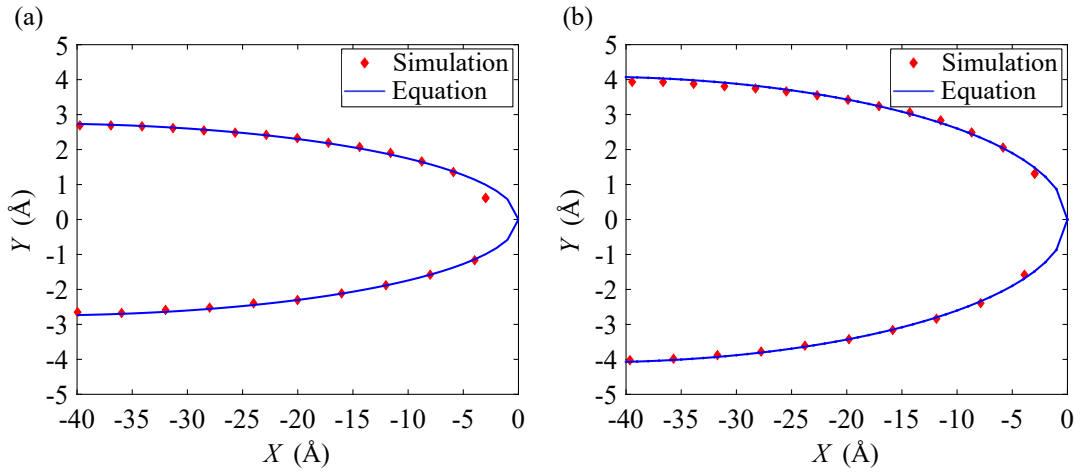

Fig. 8. Crack opening profiles calculated by molecular dynamics simulation and Eqs. (6)-(7), where (a) is at the moment of stacking fault nucleation (16.4 ps) and (b) is at the moment of intergranular crack cleavage (17.6 ps) under the loading rate of 0.25 (0.50) GPa/ps.

$$f_1 = \frac{1}{2(C_1 + C_2)F_1(\alpha,\beta)\sigma(t)}\left[\frac{1}{N}\sum_{i=1}^{N}\frac{u_{yu}^{i}}{\sqrt{-x_i l_{CX} - x_i^2}} + \frac{1}{P}\sum_{j=1}^{P}\frac{-u_{yl}^{i}}{\sqrt{-x_j l_{CX} - x_j^2}}\right] \tag{10}$$

Fig. 9(a) and (b) provide stress intensity factors and dynamic time-dependent factors under different loading rates, respectively. As shown in Fig. 9(a), variations of stress intensity factors for intergranular crack cleavage and stacking fault nucleation with loading rate are not apparent. The calculated stress intensity factors for staking fault nucleation and intergranular crack cleavage are highly consistent with fracture mechanics concept. Stress intensity factor is an invariant that controls crack propagation. Therefore, variations of critical stresses for stacking fault formation and intergranular crack cleavage are mainly attributed to the variations of respective dynamic time-dependent factors. As depicted in Fig. 9(b), for intergranular crack cleavage, dynamic time-dependent factor decreases with the increase of loading rate, which leads to the increase of critical stress. For stacking fault nucleation when loading rate is lower than 0.40 (0.80) GPa/ps, dynamic time-dependent factor decreases as loading rate increases, which results in the increase of critical stress. When loading rate is higher than 0.45 (0.90) GPa/ps, dynamic time-dependent factor increases with further increase of loading rate, which decreases critical stress. When loading rate is between 0.40 (0.80) and 0.45 (0.90) GPa/ps, a transition state occurs, and variation of critical stress for stacking fault nucleation is influenced by fluctuation of stress intensity factor.

4.1.3. *Intergranular crack propagation characteristic*

Under different loading rates, the growth rates of crack length and the number of slip atoms can be disparate. As described in Fig. 10, the final increments of crack length and slip atom number increase with loading rate increasing. Due to the same consumption time in simulation, the growth rates of crack length and slip atom number increase with an increase in loading rate. The increments of crack length and slip atom number under the loading rate of 0.50 (1.00) GPa/ps are not shown in Fig. 10 because the result can be polluted by grain boundary activity in late simulation stage. Under the loading rates of 0.25 (0.50) GP/ps and 0.30 (0.60) GP/ps, data points are aggregated at the end. Hence, similar to intergranular crack propagation under the loading rate of 0.25 (0.50) GP/ps, intergranular crack stops cleaving, and plastic zone induced by atomic slip stops expanding at second double-teeth meshing area under the loading rate of 0.30 (0.60) GP/ps. However, under the loading rates of higher than 0.30 (0.60) GP/ps, data points are not aggregated at the end. Therefore, intergranular crack can keep cleaving, and plastic zone can keep expanding at second double-teeth meshing area. For crack propagation with a constant ductile level, the increment of crack length is proportional to the increment of plastic zone area. In Fig. 10, one can see that loading rate has almost no effect on ductile level in the early stage of intergranular crack propagation. For example, when the increment of crack length is lower than 20 Å, the variations of slip atom number under different loading rates are very similar. In particular, the increments of slip atom number when crack starts to cleave are identical. For ductile crack propagation, actual threshold stress intensity factor for crack cleavage is.

$$K_{\mathrm{G}}^{\mathrm{A}} = \sqrt{2(2\gamma + \gamma_{\mathrm{p}} - E_{\mathrm{g}})/(C_1 + C_2)} \tag{11}$$

where γ_{p} is accumulated plastic strain energy before crack cleavage. As a result, accumulated plastic strain energy is independent of loading rate. Under different loading rates, actual threshold stress intensity factors for ductile crack cleavage are identical, which is well consistent with the results shown in Fig. 9(a). Calculated threshold stress intensity factors for intergranular crack cleavage under different loading rates fluctuate within a very narrow range. Departing from the early stage of intergranular crack propagation, the effect of loading rate on ductile level becomes obvious when loading rate is lower than 0.35 (0.70) GP/ps. For example, when the increment of crack length is higher than 20 Å, intergranular crack under high loading rate has a larger number of slip atoms for the same increment of crack length. Intergranular crack propagation becomes more ductile with loading rate increasing. However, when

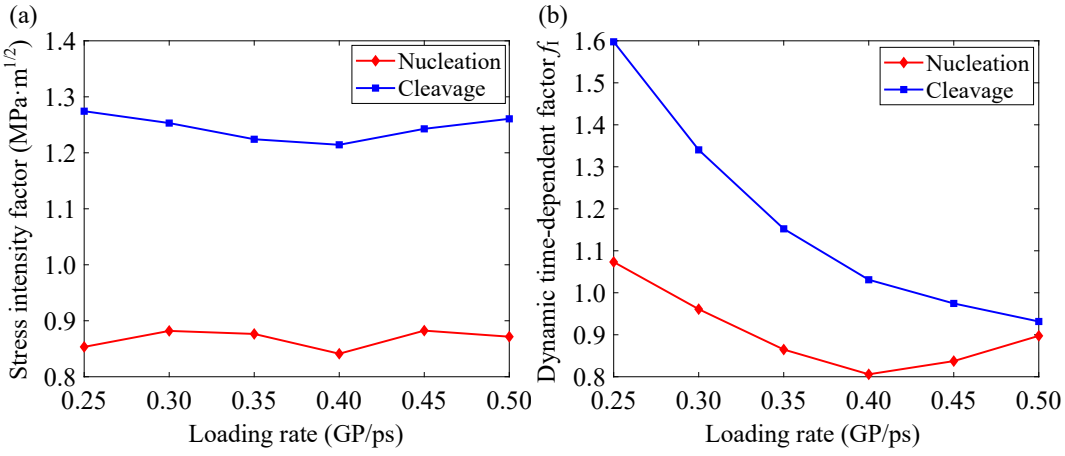

Fig. 9. Stress intensity factors and dynamic time-dependent factors under different loading rates.

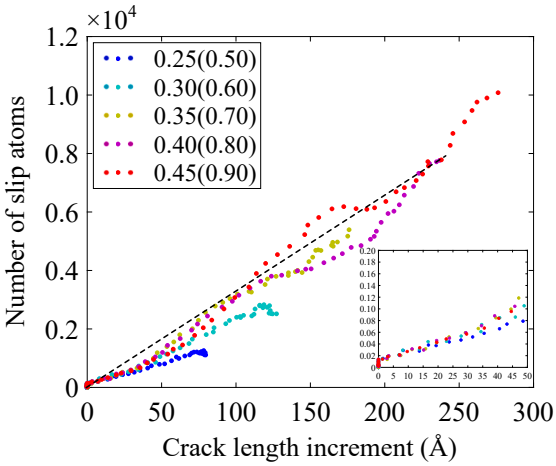

Fig. 10. Intergranular crack propagation characteristics under different loading rates.

loading rate is higher than 0.35 (0.70) GP/ps, the ratios of the increment of crack length to that of slip atom number under different loading rates are almost similar in most stages, especially at the end of simulation. The ductile level of intergranular crack propagation no longer varies obviously with further increase of loading rate.

4.2. Effect of contact ratio on intergranular crack propagation

Contact ratio is a key parameter of gear design and determines the distributions of double-teeth and single-tooth meshing areas. With a decrease in contact ratio, single-tooth meshing area increases, and heavy loading effect becomes more obvious. To identify the effect of contact ratio on intergranular crack propagation, five comparative simulations are carried out under the same loading rate of 0.35 (0.70) GPa/ps at double-teeth (single-tooth) meshing area. In these five comparative simulations, contact ratios are 3/2, 25/16, 5/3, 25/14, and 25/13.

4.2.1. Engineering stress–strain behavior

Fig. 11 describes the engineering stress–strain behaviors of cracked bicrystal model under different contact ratios. Similar to Fig. 5, these engineering stress–strain curves also overlap in their quasi-linear parts. When each engineering stress–strain curve starts to deviate from its quasi-linear part, bicrystal model can also be seen to be subjected to yielding. With a decrease in contact ratio, the yield stress of bicrystal model increases. After deviating from quasi-linear part, bicrystal model is subjected to plastic deformation. When contact ratio is higher than 25/14, strengthening process can be clearly observed, and stress takes a long time to reach its maximum value after stress–strain curve deviates from quasi-linear part. However, when contact ratio is lower than 5/3, strengthening process cannot be clearly observed, and stress soon reaches its maximum value after stress–strain curve deviates from quasi-linear part. Although bicrystal model undergoes significant strengthening when contact ratio is higher than 25/14, ultimate strength can still increase with a decrease in contact ratio.

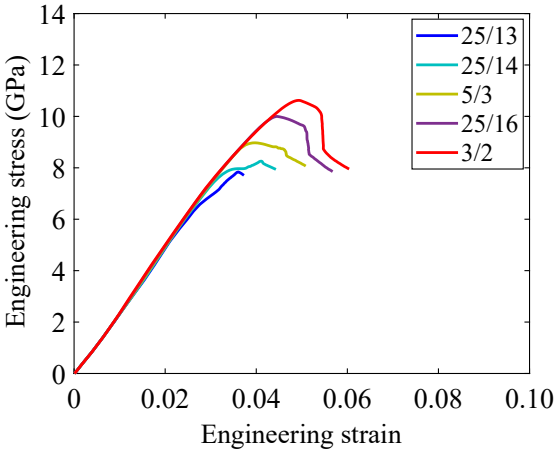

Fig. 11. Effect of contact ratio on engineering stress–strain behavior.

4.2.2. Early crack propagation and its correlation with yielding

To identify the effect of contact ratio on early crack propagation, Fig. 12 shows the variations of critical stresses for stacking fault nucleation and intergranular crack cleavage with contact ratio. When contact ratio is higher than 5/3, critical stress for stacking fault nucleation increases with a decrease in contact ratio. When contact ratio is lower than 5/3, critical stress for stacking fault nucleation decreases with further decrease of contact ratio. Variation of critical stress for stacking fault nucleation is very different from that of yield stress. Besides, critical stress for stacking fault nucleation is always lower than yield stress. With contact ratio decreasing, the difference between critical stress for stacking fault nucleation and yield stress increases. Gears are very dangerous under lower contact ratios. Unlike the variation of critical stress for stacking fault nucleation, contact ratio at the transition of critical stress for intergranular crack cleavage is 25/16. When contact ratio is higher than 25/16, critical stress for intergranular crack cleavage increases with a decrease in contact ratio. When contact ratio is lower than 25/16, critical stress for intergranular crack cleavage decreases with further decrease of contact ratio. The curve of critical stress for intergranular crack cleavage intersects with that of yield stress when contact ratio is 5/3. When contact ratio is higher than 5/3, critical stress for intergranular crack cleavage is higher than yield stress, and intergranular crack cleaves after bicrystal model yields. However, when contact ratio is lower than 5/3, critical stress for intergranular crack cleavage is lower than yield stress, and intergranular crack cleaves before bicrystal model yields. The difference between critical stress for intergranular crack cleavage and yield stress also increases with contact ratio decreasing. Compared with yield stress, the variations of critical stresses for stacking fault formation and intergranular crack cleavage put forward higher requirements for the safety design of gears with small contact ratios.

To reveal the mechanisms of the variations of critical stresses for stacking fault nucleation and intergranular crack cleavage with contact ratio, dynamic stress intensity factors under different contact ratios are calculated first based on crack opening profile. As depicted in Fig. 13 (a), critical stress intensity factors for stacking fault nucleation and intergranular crack cleavage fluctuate within a narrow range. As a consequence, the variations of critical stresses for stacking fault nucleation and intergranular crack cleavage are mainly attributed to the variations of respective dynamic time-dependent factors. As depicted in Fig. 13(b), for stacking fault nucleation under the contact ratios of higher than 5/3, dynamic time-dependent factor decreases as contact ratio decreases, which increases critical stress. For stacking fault nucleation under the contact ratios of lower than 5/3, dynamic time-dependent factor increases with further decrease of contact ratio, which leads to a decrease in critical stress. For intergranular crack cleavage under the contact ratios of higher than 25/16, dynamic time-dependent factor decreases with a decrease in contact ratio, which results in the increase of critical stress. For intergranular crack cleavage under the contact ratios of lower than 25/16, dynamic time-dependent factor increases with further decrease of contact ratio, which leads to a decrease in critical stress.

4.2.3. Intergranular crack propagation characteristic

As described in Fig. 14, the final increments of crack length and slip atom number increase with contact ratio decreasing. Due to the same consumption time in simulation, the growth rates of crack length and slip atom number increase with a decrease in contact ratio. However, contact ratio has almost no effect on ductile level in the early stage of intergranular crack propagation. In particular, under different contact ratios, the increments of slip atom number when crack starts to cleave are the same. Hence, contact ratio has no effect on accumulated plastic strain energy before intergranular crack cleavage. Actual threshold stress intensity factor is independent of contact ratio, which is consistent well with the results shown in Fig. 13(a). Departing from the early stage of intergranular crack propagation, the relationships between the increments of crack length and slip atom number under different contact ratios seem to obey the same rule before second double-teeth meshing, as shown by solid curve with an arrow in Fig. 14. The effect of contact ratio on ductile level of intergranular crack propagation cannot be clearly observed before second double-teeth meshing. When gear enters second double-teeth meshing, the relationship between the increments of crack length and slip atom number deviates from the solid curve with an arrow. The ductile level of intergranular crack propagation decreases with cleavage at the beginning of second double-

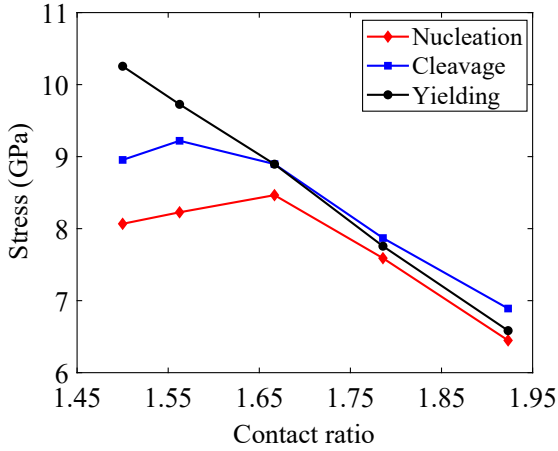

Fig. 12. Variations of yield stress, critical stress for intergranular crack cleavage, and critical stress for stacking fault nucleation with contact ratio.

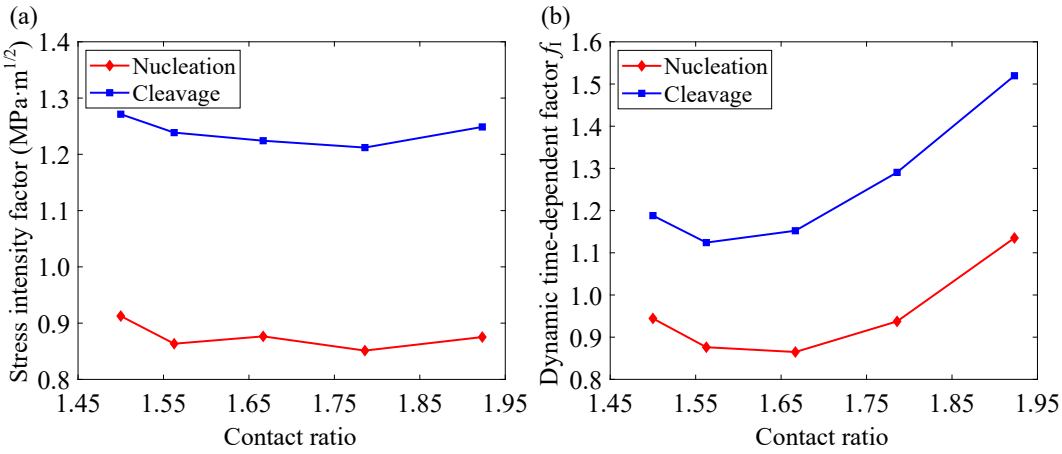

Fig. 13. Stress intensity factors and dynamic time-dependent factors under different contact ratios.

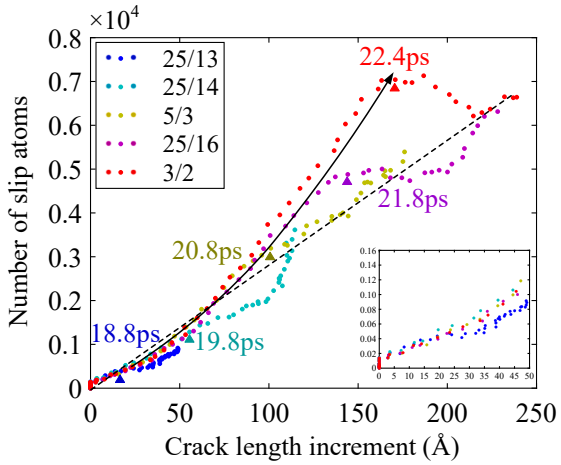

Fig. 14. Intergranular crack propagation characteristics under different contact ratios.

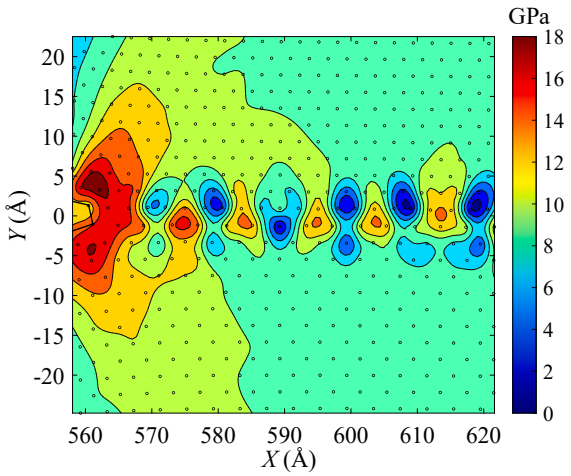

Fig. A1. Normal stress field at crack tip in bicrystal at 16.5 ps, where the calculation of normal stress can refer to a previous study [32].

teeth meshing. Afterward, the ductile level of intergranular crack propagation increases with cleavage again to follow the tendency of solid curve with an arrow. With contact ratio decreasing, the decrease of ductile level at the beginning of second double-teeth meshing becomes more evident. Under the contact ratio of 3/2, transformation from ductile to brittle propagation can be observed at the beginning of second double-teeth meshing. No matter how the ductile level varies at second double-teeth meshing area, the ratios of the increments of crack length to that of slip atom number under different contact ratios are very close at the end. Hence, the effect of contact ratio on ductile level can only exist at the beginning of second double-teeth meshing, and disappears at the end. Although the growth rates of crack length and slip atom number increase with a decrease in contact ratio, the effect of contact ratio on the ductile level of intergranular crack propagation is not obvious.

5. Conclusions

In this work, molecular dynamics simulations are carried out to identify the atomistic scale behaviors of intergranular crack propagation along twist grain boundary in bcc iron under dynamic loading rate with rectangular fluctuation. The effects of driving force and contact ratio are fully discussed. Main work and conclusions are summarized below:

(1) Intergranular crack propagation along twist grain boundary depends on resistance against both brittle crack cleavage and plastic behavior nucleation in two monocrystal portions. Grain boundary has little effect on the threshold for plastic behavior nucleation, but can significantly decrease the threshold for brittle crack cleavage. Since the threshold for brittle crack cleavage is higher than that for stacking fault nucleation in lower monocrystal portion but lower than that for edge dislocation nucleation in upper monocrystal portion, only stacking faults can be observed, and edge dislocations are suppressed by crack cleavage. Inherent ductile propagation way is only attributed to stacking faults in lower monocrystal portion.
(2) Under heavy load during single-tooth meshing, intergranular crack cleaves rapidly along twist grain boundary. Compared with crack propagation in monocrystal, intergranular crack can absorb more energy to form new surfaces. Under slight load during second double-teeth meshing, intergranular crack stops cleaving. At the same time, stacking faults shrink gradually, and anti-twinning bands extend along anti-twinning direction. Unlike crack propagation in monocrystal, plastic strain energy cannot contribute to new surface formation and is dissipated by atomic slip along anti-twinning direction. Intergranular crack propagation is in the weakest ductile way when compared with crack propagation in monocrystal cases. Twist grain boundary can significantly reduce the ductility of crack propagation.
(3) Yield stress, critical stress for stacking fault nucleation, and critical stress for intergranular crack cleavage vary with driving force and contact ratio. With an increase in driving force or a decrease in contact ratio, differences between yield stress and critical stresses for stacking fault nucleation and crack cleavage become more apparent. Compared with yield stress, critical stresses for stacking fault nucleation and crack cleavage put forward higher requirements for the safety design of gears with small contact ratios or under heavy load working conditions. The variations of critical stress for stacking fault nucleation and critical stress for crack cleavage are attributed to the variations of time-dependent factors. The variations of time-dependent factors provide a good reference for gear safety design.
(4) In the early stage of intergranular crack propagation, the effects of driving force and contact ratio on the growths of crack length and plastic zone are not obvious. Accumulated plastic strain energy before intergranular crack cleavage is independent of driving force and contact ratio. Under different driving forces or contact ratios, threshold stress intensity factors for ductile cleavage are identical. Departing from the early stage of intergranular crack propagation, the growth rates of crack length and plastic zone increase significantly with an increase in driving force or decrease in contact ratio. However, the final ductile level of intergranular crack propagation cannot vary with contact ratio and large driving force. The effect of contact ratio on the ductile level of intergranular crack propagation can only exist at the beginning of second double-teeth meshing, and disappears at the end. Driving force can affect the ductile level of intergranular crack propagation only when it is small.

Growth rate with rectangular fluctuation is the typical feature of stress on gear tooth root. By applying dynamic load, this work can be used to reveal the mechanism of gear failure at atomistic scale. However, this work only considers the twist grain boundary formed by two single crystals with significant differences in plastic behavior nucleation and crack growth resistance. Further studies will discuss the effect of twist angle on intergranular crack propagation behavior to systematically reveal gear failure mechanism at atomistic scale.

CRediT authorship contribution statement

Zhifu Zhao: Conceptualization, Data curation, Formal analysis, Funding acquisition, Investigation, Methodology, Project administration, Resources, Software, Validation, Visualization, Writing – original draft, Writing – review & editing. **Babak Safaei:** Investigation, Writing – original draft, Writing – review & editing. **Yanfei Wang:** Writing – original draft, Writing – review & editing, Investigation. **Yanwei Liu:** Writing – original draft, Writing – review & editing, Investigation. **Fulei Chu:** Supervision, Writing – original draft, Writing – review & editing, Funding acquisition. **Yueguang Wei:** Funding acquisition, Supervision, Writing – original draft, Writing – review & editing.

Declaration of Competing Interest

The authors declare that they have no known competing financial interests or personal relationships that could have appeared to influence the work reported in this paper.

Data availability

Data will be made available on request.

Acknowledgments

The authors are grateful to National Postdoctoral Program for Innovative Talents (Grant No. BX20200007); China Postdoctoral Science Foundation (Grant No. 2020M670035); National Natural Science Foundation of China (Grant Nos. 51335006, 11890681, 12032001); and High-performance Computing Platform of Peking University for supporting this research.

Appendix A

Normal stress field at crack tip in bicrystal before stacking fault nucleation.

References

[1] Ribrant J, Bertling LM. Survey of failures in wind power systems with focus on swedish wind power plants during 1997–2005. IEEE Trans Energy Convers 2007;22:167–73.
[2] Podrug S, Jelaska D, Glodez S. Influence of different load models on gear crack path shapes and fatigue lives. Fatigue Fract Engng Mater Struct 2008;31:327–39.
[3] S. Kubo, M. Misaki, Molecular dynamics simulation of influence of grain boundary on near-threshold fatigue crack growth, In: H. Kitagawa, Y. Shibutani, (eds) IUTAM Symposium on Mesoscopic Dynamics of Fracture Process and Materials Strength. Solid Mechanics and its Applications. Springer, Dordrecht. 115 (2004) 311–320.
[4] Yu ZM, Yin DF. A theoretical method to calculate the surface free energies of crystals. Acta Phys Sin 2005;54(8):3822–30.
[5] H. Tada, P.C. Paris, G.R. Irwin, The Stress Analysis of Cracks Handbook (third ed.), ASME Press, New York (2000).
[6] Rice JR. Dislocation nucleation from a crack tip: an analysis based on the Peierls concept. J Mech Phys Solids 1992;40(2):239–71.
[7] Tadmor EB, Hai S. A Peierls criterion for the onset of deformation twinning at a crack tip. J Mech Phys Solids 2003;51(5):765–93.
[8] Ersland CH, Vatne IR, Thaulow C. Atomistic modeling of penny-shaped and through-thickness cracks in bcc iron. Model Simul Mater Sci Eng 2012;20(7):075004.
[9] Vatne IR, Stukowski A, Thaulow C, Østby E, Marian J. Three-dimensional crack initiation mechanisms in bcc-Fe under loading modes I, II and III. Mater Sci Eng A-Struct Mater Prop Microstruct Process 2013;560:306–14.
[10] Daw MS, Foiles SM, Baskes MI. An atomic model of crack tip deformation in aluminum using an embedded atom potential. J Mater Res 1990;5(2):313–24.
[11] Qi Y, Wu WP, Chen YB, Chen MX. Crystal orientation dependence of crack growth and stress evolution in single crystal nickel: a molecular dynamics simulation-based cohesive zone model. RSC Adv 2015;5(81):65942–8.
[12] Skogsrud J, Thaulow C. Effect of crystallographic orientation on nanomechanical modelling of an iron single crystal cracked cantilever beam. Mater Sci Eng A-Struct Mater Prop Microstruct Process 2017;685:274–83.
[13] Zhao ZF, Qin ZY, Chu FL. Atomistic scale fracture behavior of the bcc iron with 110 crack under dynamic rectangular loading rate. Comput Mater Sci 2019;158:178–91.
[14] Zhao ZF, Qin ZY, Chu FL. Asymmetrical propagation mechanism of the crack in bcc iron. Comput Mater Sci 2020;172:109341.
[15] Shi XS, Feng XT, Zhang BW, Sun Y, He WF, Zhou LC. Research on microstructure deformation mechanism of crack tip in titanium under tension along different orientations. Mol Simul 2020;46:440–7.
[16] Singh SK, Parashar A. Atomistic simulations to study crack tip behavior in multi-elemental alloys. Engng Fract Mech 2021;243:107536.
[17] Wu Z, Curtin WA. Brittle and ductile crack-tip behavior in magnesium. Acta Mater 2015;88:1–12.
[18] Farkas D, Swygenhoven HV, Derlet PM. Intergranular fracture in nanocrystalline metals. Phys Rev B 2002;66(6):060101.
[19] Latapie A, Farkas D. Molecular dynamics investigation of the fracture behavior of nanocrystalline α–Fe. Phys Rev B 2004;69(13):134110.
[20] Zhao ZF, Chu FL, Wei YG. Atomistic scale behaviors of crack propagation in nanocrystalline bcc iron. Mater Sci Eng A-Struct Mater Prop Microstruct Process 2021;809:140948.
[21] Cheng Y, Jin ZH, Zhang YW, Gao H. On intrinsic brittleness and ductility of intergranular fracture along symmetrical tilt grain boundaries in copper. Acta Mater 2010;58:2293–9.
[22] Adlakha I, Tschopp MA, Solanki KN. The role of grain boundary structure and crystal orientation on crack growth asymmetry in aluminum. Mater Sci Eng A-Struct Mater Prop Microstruct Process 2014;618:345–54.
[23] Zhou YG, Yang ZY, Lu ZX. Dynamic crack propagation in copper bicrystals grain boundary by atomistic simulation. Mater Sci Eng A-Struct Mater Prop Microstruct Process 2014;599:116–24.
[24] Shimokawa T, Tsuboi M. Atomic-scale intergranular crack-tip plasticity in tilt grain boundaries acting as an effective dislocation source. Acta Mater 2015;87:233–47.
[25] Jung SP, Kwon Y, Lee CS, Lee BJ. Influence of hydrogen on the grain boundary crack propagation in bcc iron: A molecular dynamics simulation. Comput Mater Sci 2018;149:424–34.
[26] Chung H, Cho M. A molecular dynamics study on the biased propagation of intergranular fracture found in copper STGB. J Mech Sci Technol 2018;32(11):5351–61.
[27] Nishimura K, Miyazaki N. Molecular dynamics simulation of crack growth under cyclic loading. Comput Mater Sci 2004;31:269–78.
[28] Machová A, Pokluda J, Uhnáková A, Hora P. 3D atomistic studies of fatigue behavior of edge crack (001) in bcc iron loaded in mode I and II. Int J Fatigue 2014;66:11–9.
[29] Ma L, Xiao SF, Deng HQ, Hu WY. Molecular dynamics simulation of fatigue crack propagation in bcc iron under cyclic loading. Int J Fatigue 2014;68:253–9.
[30] Yasbolaghi R, Khoei AR. Micro-structural aspects of fatigue crack propagation in atomistic-scale via the molecular dynamics analysis. Eng Fract Mech 2020;226:106848.
[31] Machová A, Ackland GJ. Dynamic overshoot in α-iron by atomistic simulations. Model Simul Mater Sci Eng 1998;6:521–42.

[32] Zhao ZF, Chu FL. Atomic behaviors of crack propagation in bcc iron under dynamic loading rate with rectangular fluctuation. Mater Sci Eng A-Struct Mater Prop Microstruct Process 2017;707:81–91.
[33] Zhao ZF, Chu FL. Dynamic meshing force and blunt effects on atomistic scale ductile-brittle behavior of the crack in bcc iron. Eng Fract Mech 2019;208:131–50.
[34] Plimpton S. Fast parallel algorithms for short-range molecular dynamics. J Comput Phys 1995;117(1):1–19.
[35] Mendelev MI, Han S, Srolovitz DJ, Ackland GJ, Sun DY, Asta M. Development of new interatomic potentials appropriate for crystalline and liquid iron. Philos Mag 2003;83(35):3977–94.
[36] Swope WC, Andersen HC, Berens PH, Wilson KR. A computer simulation method for the calculation of equilibrium constants for the formation of physical clusters of molecules: Application to small water clusters. J Chem Phys 1982;76(1):637–49.
[37] Helio T, Paulo SB, Jose PR. Structural characterization of deformed crystals by analysis of common atomic neighborhood. Comput Phys Commun 2007;177(6):518–23.
[38] Y. Murakami (Ed.), Stress Intensity Factors Handbook, 1, Pergamon Press, Oxford (1988), pp. 67–68.
[39] C.T. Sun, Z.H. Jin, Fracture Mechanics, Academic Press, Waltham (2012), pp. 42–43.